Inorganic Chemistry

Article

pubs.acs.org/IC

Electron-Deficient $Eu_{6.5}Gd_{0.5}Ge_6$ Intermetallic: A Layered Intergrowth Phase of the Gd_5Si_4- and FeB-Type Structures

Jinlei Yao, Peng Wang, and Yurij Mozharivskyj*

Department of Chemistry and Chemical Biology, McMaster University, 1280 Main Street West, Hamilton, Ontario L8S 4M1, Canada

Supporting Information

ABSTRACT: A novel electron-poor $Eu_{6.5}Gd_{0.5}Ge_6$ compound adopts the Ca_7Sn_6-type structure (space group *Pnma*, $Z = 4$, $a = 7.5943(5)$ Å, $b = 22.905(1)$ Å, $c = 8.3610(4)$ Å, and $V = 1454.4(1)$ Å^3). The compound can be seen as an intergrowth of the Gd_5Si_4-type (*Pnma*) R_5Ge_4 (R = rare earth) and FeB-type (*Pnma*) RGe compounds. The phase analysis suggests that the $Eu_{7-x}Gd_xGe_6$ series displays a narrow homogeneity range of stabilizing the Ca_7Sn_6 structure at $x \approx 0.5$. The structural results illustrate the structural rigidity of the $^2_\infty[R_5X_4]$ slabs (X = *p*-element) and a possibility for discovering new intermetallics by combining the $^2_\infty[R_5X_4]$ slabs with other symmetry-approximate building blocks. Electronic structure analysis suggests that the stability and composition of $Eu_{6.5}Gd_{0.5}Ge_6$ represents a compromise between the valence electron concentration, bonding, and existence of the neighboring EuGe and $(Eu,Gd)_5Ge_4$ phases.

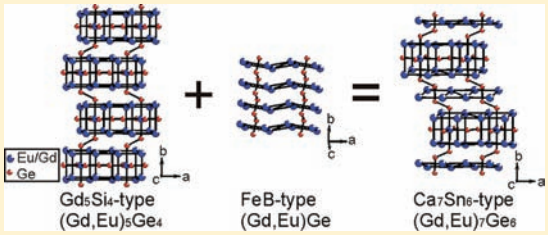

INTRODUCTION

Discovery of a giant magnetocaloric effect in $Gd_5Si_2Ge_2$ stimulates extensive studies on the relationship between the crystal structures and physical properties of the R_5X_4 family of compounds (where R = rare-earth element and X = *p*-element).[1−11] Except for the tetragonal Zr_5Si_4- (space group $P4_12_12$) and hexagonal Ti_5Ga_4-type ($P6_3/mcm$) structures, the R_5X_4 phases are found to adopt one or more of the eight related structures: Sm_5Ge_4 (*Pnma*),[12,13] Gd_5Si_4 (*Pnma*),[12,13] $Gd_5Si_2Ge_2$ ($P2_1/a$),[1] Pu_5Rh_4 (*Pnma*),[5] Eu_5As_4 (*Cmca*),[11] $U_2Mo_3Si_4$ ($P2_1/c$),[9] $Gd_5Si_2Bi_2$ ($I4_1/acd$), and $Gd_5Si_{1.5}Bi_{2.5}$ ($P4_2bc$).[10] These eight layered structures are constructed from the same building block, the $^2_\infty[R_5X_4]$ slab, but with various types of interslab X−X bonds (e.g., Gd_5Si_4 in Figure 1 has all the interslab X−X bonds intact).

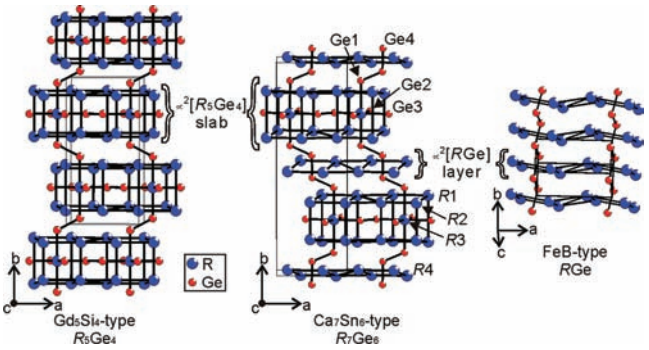

Figure 1. Crystal structure of Gd_5Si_4-type R_5Ge_4, Ca_7Sn_6-type R_7Ge_6, and FeB-type RGe (R = a mixture of Eu and Gd).

Some R_5X_4 compounds undergo structural transformations as a function of temperature, magnetic field, or pressure.[1,3,4] During such transitions, the $^2_\infty[R_5X_4]$ slabs remain intact but the interslab X−X bonds can either stretch, break, or reform, thus indicating the structural rigidity of the $^2_\infty[R_5X_4]$ slabs and flexibility of the interslab bonds.[2,5,10] These structural features encouraged us to search for new phases beyond the R_5X_4 family, what would assemble the $^2_\infty[R_5X_4]$ slabs and other symmetry-allowed building blocks into their structures. In this work, we report on the synthesis and characterization of a new series of pseudo-binary $Eu_{7-x}Gd_xGe_6$ compounds that adopt the Ca_7Sn_6 structure (*Pnma*) and display a narrow homogeneity range around the $Eu_{6.5}Gd_{0.5}Ge_6$ composition. The $(Eu,Gd)_7Ge_6$ compound, isostructural with Ca_7Sn_6, shows remarkable structural similarities to the R_5X_4 ones.

EXPERIMENTAL SECTION

Sample Preparation. The Ca_7Sn_6-type R_7Ge_6 crystal was found during the exploration of the electron-poor $Gd_{5-x}Eu_xGe_4$ phases with $x > 3$.[14] The actual composition for the crystal could not be resolved by the conventional X-ray/neutron diffraction techniques, because of the neighboring atomic numbers and large neutron cross sections of Gd and Eu.[15] Following the discovery of the R_7Ge_6 crystal, the $Eu_{7-x}Gd_xGe_6$ ($x = 0−2$) samples were prepared. The starting materials were pieces of europium (99.9+ wt %, distilled grade, Rhone Poulenc), gadolinium (99.99 wt %, distilled grade, Metal Rare Earth Limited, China), and germanium (99.9999 wt %, Alfa Aesar). Because of the high air sensitivity of europium metal, all materials were handled in an argon-filled glovebox. The surface of europium metal lumps was scraped with a file before being cut into pieces. Mixtures of each reactant based on the $Eu_{7-x}Gd_xGe_6$ stoichiometry were loaded into tantalum ampules, which were sealed by arc melting under an argon atmosphere. These ampules were heated in a high-frequency induction furnace at 1450 °C for 4 h and thereafter were subjected to 1200 °C for 15 h.

Received: December 7, 2011
Published: February 15, 2012

   dx.doi.org/10.1021/ic2026413 | *Inorg. Chem.* 2012, 51, 3172−3178

Table 1. Phase Analysis of $Eu_{7-x}Gd_xGe_6$ (x = 0−2.0) from the Rietveld Refinement of the X-ray Powder Diffraction Data[a]

x	phase type	a (Å)	b (Å)	c (Å)	V (Å^3)	phase fraction (wt %)
0	CrB (*Cmcm*)	4.72971(4)	11.2083(1)	4.11203(4)	217.987(4)	76(1)
	Cr_5B_3 (*I*4/*mcm*)	7.9895(9)	7.9895(9)	15.397(3)	982.8(2)	24.0(6)
0.25	Ca_7Sn_6 (*Pnma*)	7.6152(5)	22.993(2)	8.3854(6)	1468.3(2)	90.6(7)
	Gd_5Si_4 (*Pnma*)	7.737(2)	15.291(4)	8.020(2)	948.9(4)	8.1(3)
	CrB (*Cmcm*)	4.725(2)	11.215(4)	4.111(1)	217.8(1)	1.2(5)
0.50	Ca_7Sn_6 (*Pnma*)	7.615(1)	22.999(3)	8.381(1)	1467.8(4)	92.2(8)
	Cr_5B_3 (*I*4/*mcm*)	7.959(8)	7.959(8)	15.208(7)	963(1)	7.8(2)
0.75	Gd_5Si_4 (*Pnma*)	7.7129(9)	15.864(2)	8.148(1)	997.0(2)	58.5(5)
	CrB (*Cmcm*)	4.7149(3)	11.2011(8)	4.1048(3)	216.78(2)	41.5(3)
1.0	Gd_5Si_4 (*Pnma*)	7.6932(8)	15.742(2)	8.149(1)	986.9(2)	54.2(5)
	CrB (*Cmcm*)	4.7170(4)	11.2060(9)	4.1070(3)	217.09(3)	45.8(2)
1.3	Gd_5Si_4 (*Pnma*)	7.6728(8)	15.615(2)	8.1164(9)	972.4(2)	54.6(5)
	CrB (*Cmcm*)	4.7046(5)	11.188(1)	4.0997(4)	215.80(3)	45.4(3)
2.0	Gd_5Si_4 (*Pnma*)	7.642(1)	15.492(2)	8.097(1)	958.6(2)	74.4(6)
	CrB (*Cmcm*)	4.7136(6)	11.201(1)	4.1040(6)	216.68(5)	25.6(3)

[a]The Ca_7Sn_6-type $(Eu,Gd)_7Ge_6$, Gd_5Si_4-type $(Eu,Gd)_5Ge_4$, CrB-type (Eu,Gd)Ge, and Cr_5B_3-type $(Eu,Gd)_5Ge_3$ compounds were identified.

X-ray Analysis. The phase purity of the samples was evaluated through powder X-ray diffraction (XRD) on a PANalytical X'Pert Pro diffractometer, using Co Kα radiation. All powder XRD patterns were analyzed through Rietveld refinement, using the Rietica package.[16] A pseudo-Voigt function with the Howard asymmetry correction was used to model the peak profile, and the background was described with a polynomial function. The refinement results are gathered in Table 1. The sample with x = 0 was revealed to contain the CrB-type (*Cmcm*) (Eu,Gd)Ge compound as a major phase and the Cr_5B_3-type (*I*4/*mcm*) $(Eu,Gd)_5Ge_3$ compound as a minor phase. The samples with x = 0.25−0.50 yield the dominant Ca_7Sn_6-type $(Eu,Gd)_7Ge_6$ phase. A mixture of the Gd_5Si_4-type $(Eu,Gd)_5Ge_4$ phase with the CrB-type phase was found in the samples with x = 0.75−2.0.

Single-crystal XRD data at room temperature were obtained on a STOE IPDS II diffractometer with Mo Kα radiation. A numerical absorption correction was based on the crystal shape obtained from the optical face indexing and then performed by the program X-Shape, which was included with the STOE IPDS software package.[17] The space group was assigned on the basis of the systematic absences and the statistical analysis of the intensity distributions. Structure determination using direct methods and refinement using full-matrix least-squares on F^2 were carried out with the SHELXL package.[18,19] Because of the similar X-ray scattering factor of Gd and Eu, attempts to fix Gd on a specified R-site had little or no improvement on the refinements. Considering that R/R′ mixtures are present on all metal sites, despite of site preferences in the $(R,R')_5X_4$ phases,[20] we believe that a similar mixing occurs in R_7Ge_6 and, thus, the same Gd/Eu statistical mixtures consistent with the loaded compositions are assumed on all of the metal sites. Some details of the single-crystal data collections and refinements are listed in Table 2. Atomic position parameters and isotropic displacement parameters are given in Table 3, and the selected bond distances are gathered in Table 4. Further details of the crystal structure investigated are available from the Fachinformationszentrum Karlsruhe, 76344 Eggenstein-Leopoldshafen, Germany, on quoting the depository number CSD-423666 ($Eu_{6.5}Gd_{0.5}Ge_6$).

Magnetic Measurements. Magnetization in a zero-field-cooled mode for the polycrystalline $Eu_{6.5}Gd_{0.5}Ge_6$ sample was measured on a Quantum Design SQUID magnetometer in the temperature range of 2−350 K under a 100 Oe magnetic field. The Curie temperature (T_C) was determined as a maximum on the dM/dT curve. The Weiss temperature (θ) and the effective magnetic moment (μ_R) of R (where R is a mixture of Eu and Gd) were obtained by fitting the paramagnetic data to the Curie−Weiss law. The isothermal magnetizations at various temperatures were measured in the fields of up to 5 T.

Table 2. Crystallographic Data for $Eu_{6.5}Gd_{0.5}Ge_6$ as Obtained from the Single-Crystal X-ray Diffraction at Room Temperature[a]

parameter	value
empirical formula[b]	$Eu_{6.5}Gd_{0.5}Ge_6$
structure type	Ca_7Sn_6 (*Pnma*, No. 62)
a	7.5943(5) Å
b	22.905(1) Å
c	8.3610(4) Å
volume, V	1454.4(1) Å^3
Z	4
θ range	2.59°−34.65°
number of data/parameters	3076/65
goodness-of-fit on F^2	0.783
R_1/wR_2 [$I > 2\sigma(I)$]	0.0417/0.0269
extinction coefficient	0.000073(6)
peak	2.240 e/Å^3
hole	−2.704 e/Å^3

[a]Using Mo Kα radiation and a STOE IPDS II diffractometer. [b]The formula is assigned according to the loaded composition.

Electronic Structure Calculations. In order to understand the R-site occupation and structural stability, the electronic structures of the hypothetical "Eu_6GdGe_6" and "Eu_7Ge_6" compounds were calculated with a tight-binding, linear-muffin-tin orbital method with the atomic sphere approximation (TB−LMTO−ASA),[21] using the Stuttgart program.[22] The structural parameters of Eu_6GdGe_6 and Eu_7Ge_6 were taken from the structural data of $Eu_{6.5}Gd_{0.5}Ge_6$, which are shown in Tables 2 and 3. For the calculations of Eu_6GdGe_6, the symmetry was reduced to $Pn2_1a$ to allow Gd to occupy one-half of either the R1, R2, or R4 sites. The R1 (8*d*) site was split into two sites, R1A (4*a*) and R1B (4*a*), and so were the R2 and R4 sites in the $Pn2_1a$ symmetry. Gd was placed either into the R1A, R2A, R3, or R4A sites, and the resulting models were designated as **1**, **2**, **3**, and **4**, respectively. The atomic coordinates are given in Table S1 in the Supporting

dx.doi.org/10.1021/ic2026413 | Inorg. Chem. 2012, 51, 3172−3178

Table 3. Atomic Coordinates and Isotropic Displacement Parameters (U_{eq}) for $Eu_{6.5}Gd_{0.5}Ge_6$ as Obtained from the Single-Crystal X-ray Diffraction

atom	site	x	y	z	U_{eq} (Å^2)
R1[a]	8*d*	0.14127(4)	0.14086(2)	0.31835(6)	0.01406(9)
R2[a]	8*d*	0.02200(4)	0.66231(2)	0.17991(5)	0.01016(8)
R3[a]	4*c*	0.30874(6)	0.2500	0.02366(7)	0.0150(1)
R4[a]	8*d*	0.33987(4)	0.51891(2)	0.17654(5)	0.01161(8)
Ge1	8*d*	0.19269(9)	0.59769(4)	0.4695(1)	0.0123(2)
Ge2	4*c*	0.1844(1)	0.2500	0.6032(2)	0.0169(3)
Ge3	4*c*	0.4126(1)	0.2500	0.3842(1)	0.0147(3)
Ge4	8*d*	0.00365(9)	0.05342(4)	0.0391(1)	0.0111(2)

[a]R is defined as a statistical mixture of europium and gadolinium (Eu:Gd = 6.5:0.5).

Table 4. Interatomic Distances in $Eu_{6.5}Gd_{0.5}Ge_6$

atoms[a]	distance (Å)	atoms[a]	distance (Å)
Ge1−Ge4 (×8)	2.586(1)	Ge4−R1 (×8)	3.249(1)
		R1 (×8)	3.6063(9)
Ge2−Ge3 (×4)	2.521(2)	R2 (×8)	3.100(1)
		R4 (×8)	3.1534(9)
Ge4−Ge4 (×4)	2.534(1)	R4 (×8)	3.2534(9)
		R4 (×8)	3.2683(8)
Ge1−R1 (×8)	3.2492(9)	R4 (×8)	3.3506(9)
R1 (×8)	3.328(1)		
R2 (×8)	3.1196(9)	R1−R1 (×8)	3.9654(5)
R2 (×8)	3.1630(8)	R2 (×8)	3.9899(6)
R3 (×8)	3.5180(9)	R2 (×8)	4.3742(7)
R4 (×8)	3.192(1)	R2 (×8)	4.4019(7)
R4 (×8)	3.2410(9)	R3 (×8)	3.7333(6)
R4 (×8)	3.4534(9)	R3 (×8)	3.7910(5)
		R4 (×8)	4.0978(6)
Ge2−R1 (×8)	3.468(1)	R4 (×8)	4.1319(6)
R2 (×8)	3.0687(8)	R4 (×8)	4.3166(6)
R2 (×8)	3.127(1)		
R3 (×4)	3.044(1)	R2−R2 (×8)	3.9739(5)
R3 (×4)	3.640(1)	R2 (×4)	4.0173(6)
		R3 (×8)	3.6388(6)
Ge3−R1 (×8)	3.2862(8)	R3 (×8)	3.7346(6)
R1 (×8)	3.4830(9)	R4 (×8)	3.7606(6)
R2 (×8)	3.224(1)	R4 (×8)	4.0763(5)
R3 (×4)	3.105(1)		
R3 (×4)	3.116(1)	R4−R4 (×4)	3.9218(6)
		R4 (×8)	3.9909(5)
		R4 (×8)	4.4822(6)

[a]The number of bonds per unit cell is given in parentheses.

Information. Exchange and correlation were treated by the local density approximation.[23] All relativistic effects except spin−orbit coupling were taken into account, using a scalar relativistic approximation.[24] In the ASA method, space is filled with overlapping Wigner−Seitz (WS) atomic spheres whose radii were obtained by requiring the overlapping potential to be the best possible approximation to the full potential. No empty spheres were needed to achieve convergence. In the four models of Eu_6GdGe_6, the WS radii of R1A(B), R2A(B), R3, R4A(B), Ge1, Ge2, Ge3, and Ge4 were fixed at 2.21, 2.07, 2.05, 2.15, 1.51, 1.45, 1.45, and 1.45 Å, respectively. The WS radii employed for the Eu_7Ge_6 calculations are as follows: Eu = 2.04−2.21 Å and Ge = 1.45−1.51 Å. The basis sets included 6*s*, 6*p*, and 5*d* orbitals for Eu/Gd, and 4*s*, 4*p*, and 4*d* orbitals for Ge. The Eu/Gd 6*p* and Ge 4*d* orbitals were treated by the Löwdin downfolding technique.[21,22] The Eu atom was treated as a divalent cation, which is supported by the structural analysis and magnetic measurements. The half-filled Eu and Gd 4*f* orbitals were treated as core states. The self-consistent charge density was obtained using 128 irreducible *k*-points in the first Brillouin zone. The tetrahedron method was performed to calculate the electronic density of states (DOS) and crystal orbital Hamilton population (COHP).[25]

RESULTS AND DISCUSSION

Synthesis and Structural Features. The Rietveld refinements of the powder XRD data for $Eu_{7-x}Gd_xGe_6$ (x = 0−2.0) showed that two samples with x = 0.25 and 0.50 had the major phase isostructural with Ca_7Sn_6 (Table 1). No such phase was seen in the pure Eu_7Ge_6 sample or in the samples with $x \geq 0.75$. Considering the noticeably larger ionic radius of Eu^{2+} (1.17 Å for 6−coordinate environment) than that of Gd^{3+} (0.938 Å),[26] one expects to see a larger unit cell for the sample with x = 0.25 than that for x = 0.50, because of a greater Eu loading amount. However, the Ca_7Sn_6-type phases in both the samples have almost identical unit-cell volumes—1468.3(2) Å^3 for x = 0.25 vs 1467.8(4) Å^3 for x = 0.50 (Table 1)—indicating very close experimental Eu/Gd ratios. Therefore, we can conclude that the Ca_7Sn_6-type $Eu_{7-x}Gd_xGe_6$ phase survives in a narrow compositional range at $x \approx 0.50$, and we will focus our discussion on the $Eu_{6.5}Gd_{0.5}Ge_6$ phase. Hitherto, the Ca_7Sn_6-type structure has been found in only two binaries, i.e., Ca_7Sn_6[27] and Ca_7Ge_6.[28] $Eu_{6.5}Gd_{0.5}Ge_6$ is the first magnetic pseudo-binary to adopt this structure.

The $Eu_{6.5}Gd_{0.5}Ge_6$ compound displays a significant structural similarity to the R_5X_4 layered structures. The structure can be viewed as an intergrowth of the $^2_\infty[R_5Ge_4]$ slabs and $^2_\infty[RGe]$ layers along the *b*-axis (see Figure 1). The $^2_\infty[R_5Ge_4]$ slabs are interconnected by zigzag Ge_4 tetramers. The two building blocks share the same planar R 3^2434 nets (see Figure 2);

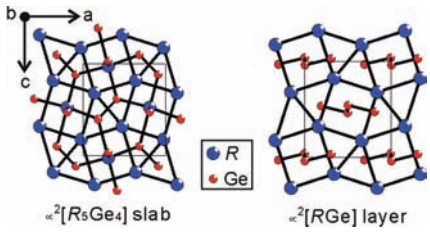

Figure 2. Projections of two building fragments, the $^2_\infty[R_5Ge_4]$ slab and $^2_\infty[RGe]$ layer, in R_7Ge_6 along the *b*-axis. The two fragments contain the eclipsed 3^2434 nets formed by the R atoms. (R is a mixture of Eu and Gd.)

therefore, it is not surprising that they can be incorporated into one structure. In the $^2_\infty[R_5Ge_4]$ slab, the two adjacent R 3^2434 nets are staked in an eclipsed fashion, which creates cubic and trigonal prismatic voids. R3 atoms occupy the cubic holes, while Ge2/Ge3 atoms occupy all trigonal prismatic holes. In the $^2_\infty[RGe]$ layer, Ge1/Ge4 atoms cap the R triangle and rectangular centers. The Ge−Ge bonds within the Ge_4 tetramer are 2.534(1) and 2.586(1) Å (Table 4), which indicate their strong covalent character and compare well with the data reported for Ge single bonds in $EuGe_2$,[29] Gd_5Si_4-type $(R,A)_5Ge_4$ (R = rare earth, A = alkaline earth),[6−8] and $DyGe_3$.[30]

The conventional diffraction techniques could not establish the site occupation by the Eu and Gd atoms. However, as shown for the R_5X_4 systems,[20] analysis employing the geometric and electronic considerations may shed light on the R-site occupation. First, the local coordination environments of the four R-sites of $Eu_{6.5}Gd_{0.5}Ge_6$ are analyzed. The R1

dx.doi.org/10.1021/ic2026413 | Inorg. Chem. 2012, 51, 3172−3178

site is surrounded by 10 R and 7 Ge atoms; the R2 site is coordinated by 10 R and 6 Ge atoms; the coordination polyhedron around R3 can be seen as a combination of a distorted R cube and a Ge octahedron; and the R4 site is surrounded by 10 R and 7 Ge atoms (see Figure 3). One can

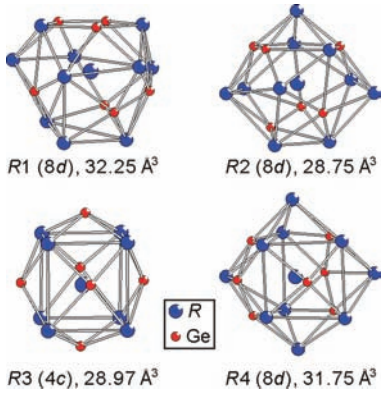

Figure 3. Coordination polyhedral around the four rare-earth sites of $Eu_{6.5}Gd_{0.5}Ge_6$. The site volume of the Wigner–Seitz cells is indicated.

see that the coordination polyhedral around the R1, R2, and R3 sites exhibit considerable similarities to the corresponding R-sites of R_5X_4,[20] because these three R-sites belong to the same building unit, the $^2_\infty[R_5X_4]$ slab, in both structures. A subtle difference between these two structures lies in the site size, i.e., the slab-centered R3 site of R_5X_4 has the tightest environment, whereas the slab-surface R2 site of $Eu_{6.5}Gd_{0.5}Ge_6$ has the smallest site volume (28.75 Å^3), as calculated by DIDO95.[31] The smaller Gd atom, as compared to Eu (the Shannon radius order of Gd^{3+} (0.938 Å) < Eu^{3+} (0.947 Å) < Eu^{2+} (1.17 Å) for six-coordinate environments[26]), is expected to prefer the smallest R2 site. The average R–Ge bond lengths are, respectively, 3.381(1) Å, 3.134(1) Å, 3.324(1) Å, and 3.273(1) Å for the R1, R2, R3, and R4 sites, while these sites have the average R–R distances of 4.0767(6), 3.9728(7), 3.7245(6), and 4.1251(6) Å, respectively. Obviously, the R2 site has the shortest R–Ge bonds, whereas the R3 site shows the shortest R–R bonds.

The metal-site occupation in intermetallics can also be considered from the perspective of electronic effects. The atoms with more electonegativy tend to occupy the sites with the larger Mulliken population.[32] In the TB-LMTO-ASA calculations, the Mulliken population can be treated as the integrated DOS (IDOS) in a semiempirical way.[9] For the calculations of the hypothetic "Eu_7Ge_6" phase, the IDOS for the R1, R2, R3, and R4 sites are 2.45, 2.58, 2.08, and 2.48, respectively. Since Gd has a larger electronegativity than Eu (Allred–Rochow electronegativity of χ(Gd) = 1.11 versus χ(Eu) = 1.01),[33] the Gd atoms are expected to occupy the R2 site with the largest IDOS value. The Gd-substitution effects on the bonding and electronic structures were examined through the calculations of "Eu_6GdGe_6". The bond strength is scaled by means of the integration of crystal orbital Hamilton population (–ICOHP). The assignment of Gd at the R2 site (model **2**) yields the strongest Gd–Ge and Gd–R interactions, leading to the lowest bond energy, Sum(–ICOHP) = 58.93 eV/cell, but the Eu–Ge and Eu–Eu interations are slightly weakened in Model **2** (see Table 5). The strong bond interactions around R2 correspond to its short R–Ge and R–R bond distances. Also, the presence of Gd on the R2 site results in the lowest

Table 5. Total Electronic Energy (E_{tot}, eV/cell) and the Integration of Crystal Orbital Hamilton Population (–ICOHP) for Various Bonds in the Structural Models of Eu_6GdGe_6[a]

	Model **1**	Model **2**	Model **3**	Model **4**
bond strength (eV/cell)				
Gd–Ge	6.80	**7.67**	6.62	7.09
Gd–R	2.54	**2.69**	2.44	2.53
Eu–Ge	33.71	33.17	**34.04**	33.50
Eu–Eu	5.57	5.40	5.48	**5.65**
Ge–Ge	10.04	10.00	**10.07**	10.01
Sum(–ICOHP)	58.66	**58.93**	58.65	58.78
E_{tot} (eV/cell)	0.21	**0**	0.16	0.10

[a]The lowest-energy terms are indicated in boldface font within the table.

total electronic energy (E_{tot}); the E_{tot} values for models **1**, **3**, and **4** are, respectively, 0.21, 0.16, and 0.10 eV/cell higher than that for model **2**. Therefore, the Gd atoms are predicted to occupy the slab-surface R2 site, based on the geometric and electronic considerations.

Magnetic Properties. To understand the structural stability and bonding character of $Eu_{6.5}Gd_{0.5}Ge_6$, one must establish the oxidation state of Eu. $Eu_{6.5}Gd_{0.5}Ge_6$ (V = 1454.4(1) Å^3) displays a larger unit cell than Ca_7Ge_6 (V = 1339.2(3) Å^3),[28] implying a divalent Eu species, according to the Shannon radius order of Eu^{2+} (1.17 Å) > Ca^{2+} (1.00 Å) > Eu^{3+} (0.947 Å) > Gd^{3+} (0.938 Å).[26] This oxidation state for Eu is also verified through the magnetic data. A fit to the paramagnetic data using the Curie–Weiss law yielded an effective magnetic moment (μ_{eff}) of 8.24 μ_B for Eu, assuming Gd takes the theoretical moment of 7.94 μ_B (see Figure 4).

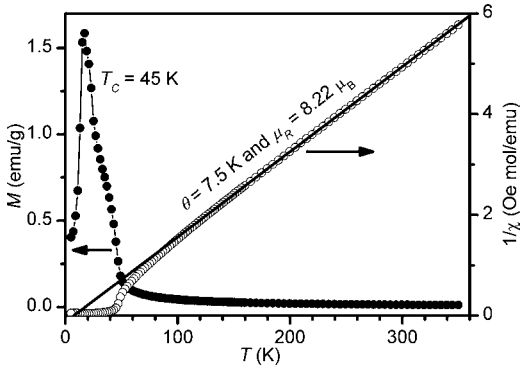

Figure 4. Temperature (T) dependence of magnetization (M) and inverse magnetic susceptibility ($1/\chi$) of $Eu_{6.5}Gd_{0.5}Ge_6$ in a magnetic field of 100 Oe. The Weiss temperature (θ) and effective magnetic moment of R (μ_R) are derived from a fit (denoted by a solid line in the figure) to the paramagnetic data, using the Curie–Weiss law. (R is a mixture of Eu and Gd.)

Since $\mu_{eff}(Eu^{2+})$ = 7.94 μ_B and $\mu_{eff}(Eu^{3+})$ = 0 μ_B for free Eu ions, the data unequivocally advocate the presence of Eu^{2+} in $Eu_{6.5}Gd_{0.5}Ge_6$. The overestimation of μ_{eff}(Eu) results from the 5*d*-electron polarization, which is frequently observed in the rare-earth intermetallics.[34,35]

The magnetic properties of $Eu_{6.5}Gd_{0.5}Ge_6$ were studied further by measuring its isothermal magnetization at various temperatures (see Figure 5). The magnetization at low temperatures, such as at 2 K, is not saturated up to 5 T and

dx.doi.org/10.1021/ic2026413 | Inorg. Chem. 2012, 51, 3172–3178

the measured magnetic moment is ~2.8 μ_B/R in 5 T, which is much smaller than the saturation magnetic moment of 7 μ_B for Eu^{2+}/Gd^{3+} (1 gJ = 7 μ_B). Arrott plots below the critical temperature (T_C = 45 K) display a distinct convex curvature and an absence of spontaneous magnetization (see Figure 5),

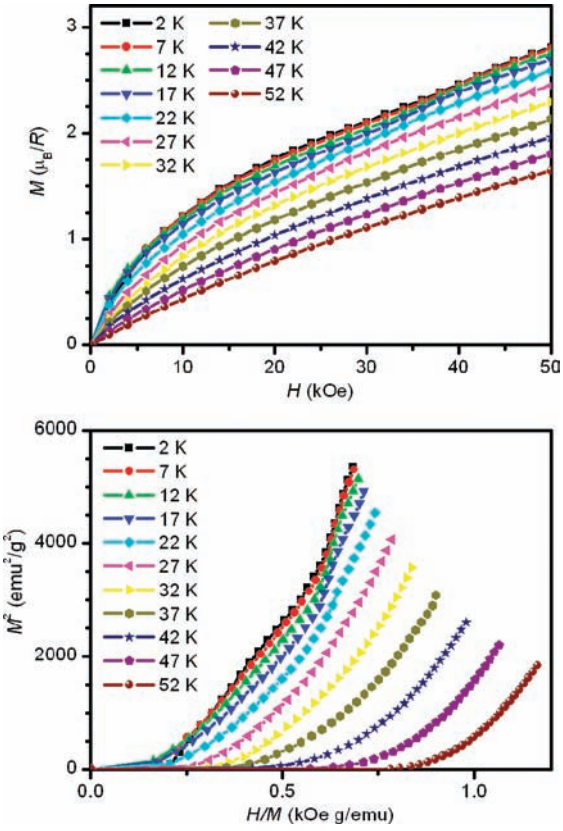

Figure 5. Magnetization (M) vs magnetic field (H) (top panel) and Arrott plots (bottom panel) of $Eu_{6.5}Gd_{0.5}Ge_6$ at various temperatures.

indicating a disordered ferromagnetic (FM) state in $Eu_{6.5}Gd_{0.5}Ge_6$.[36] It could be helimagnetic, i.e., the magnetization of the $^2_\infty[R_5Ge_4]$ slabs is spirally coupled to that of the adjacent $^2_\infty[RGe]$ layers, which was observed in some rare-earth metals and compounds with layered structures, e.g., Dy,[37] Tb_5Ge_3,[38] $Ce_2(Fe,Mn)_{17}$.[39] However, further investigations are needed to fully understand the magnetic structure of this material. At low temperatures (T < 20 K), a metamagnetic transition occurs in high fields, e.g., at ~40 kOe at 2 K and ~34 kOe at 17 K (see Figure 5). The positive slopes of the Arrott plots before and after the metamagnetic transition, as well as around T_C (see Figure 5), suggests that the magnetic transitions are second order.[40]

Electronic Structure and Bonding. One of the interesting points is what dictates the stability and composition of the $Eu_{6.5}Gd_{0.5}Ge_6$ phase. The $^2_\infty[R_5Ge_4]$ slabs and $^2_\infty[RGe]$ layers are found in the corresponding pseudo-binaries, such as $(Gd,Eu)_5Ge_4$ and (Gd,Eu)Ge (Eu_5Ge_4 is not known, but can be stabilized through Gd substitution).[14] Obviously, when these building blocks are fused, the resulting new bonds are likely to dictate the phase stability and composition, although changes to the existing interactions also can be a factor. The interactions in $Eu_{6.5}Gd_{0.5}Ge_6$ can be divided into three groups: R–R, R–Ge, and Ge–Ge. Studies on R_5Ge_4 and RGe showed that R–R and R–Ge interactions are bonding at the Fermi level (E_F) and tend to stabilize the structures, irrespective of the changes in the valence electron concentration (VEC).[5] However, the Ge–Ge bonds have significant antibonding contribution at the E_F level and are prone to cleavage, depending on the VEC.[5] We start our analysis with a qualitative approach based on the Zintl–Klemm concept with a focus on the Ge–Ge interactions.[41–43] Within this formalism, the intraslab Ge2–Ge3 dimers, located within $^2_\infty[R_5Ge_4]$ slabs are isoelectronic with halogen ones and carry a negative charge of −6. The interslab Ge1–Ge4–Ge4–Ge1 tetramer can be treated as a fragment cut from a one-dimensional $^1_\infty[Ge^{2-}]$ chain observed in EuGe and $DyGe_3$,[30,43] and it will have a configuration of $Ge1^{3-}$–$Ge4^{2-}$–$Ge4^{2-}$–$Ge1^{3-}$, with a total charge of 10−. Thus, the electronic formula of $Eu_{6.5}Gd_{0.5}Ge_6$ can be written as $(Eu^{2+})_{6.5}(Gd^{3+})_{0.5}(Ge_2^{6-})(Ge_4^{10-})(1.5\ h^+)$, suggesting presence of 1.5 holes in the valence band. Obviously, this approach is simplified, because it ignores R–R and R–Ge interactions, both of which will be significant and bonding up to the E_F level (see Figure 6). Still, the electron deficiency derived

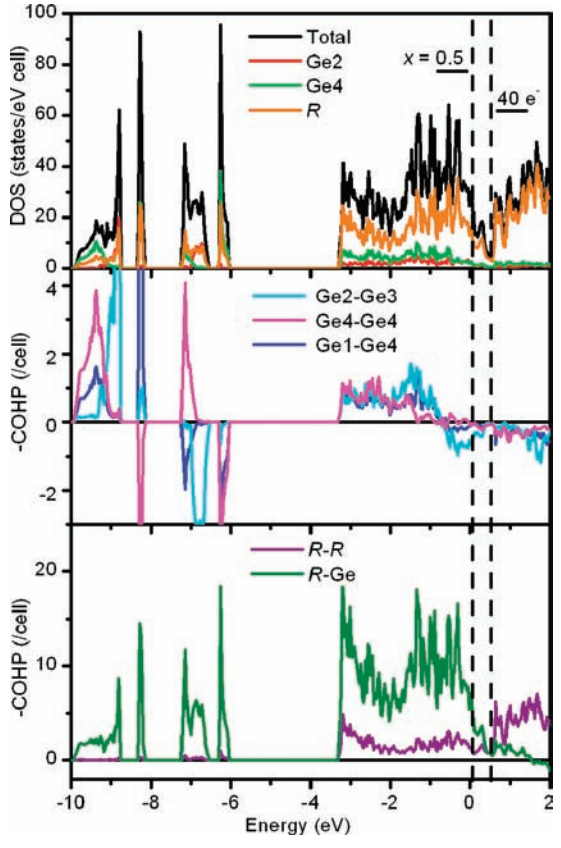

Figure 6. Density of states (DOS) and crystal orbital Hamilton population (COHP) curves for the hypothetical "Eu_7Ge_6" compound. The Ge2 and Ge3 atoms have similar projected DOS; Ge1 and Ge4 also have similar projected DOS. The vertical line at 0.07 eV is the Fermi level (E_F) for $Eu_{7-x}Gd_xGe_6$ (x = 0.5) within a rigid band approximation. The dashed line, locating at a pseudo-gap, denotes the states containing 40 valence electrons per formula unit. Interactions with −COHP > 0 and −COHP < 0 are bonding and antibonding, respectively.

by this method is reflected in the electronic structure (see Figure 6), calculated using the TB–LMTO–ASA program. A pseudo-gap at 0.61 eV corresponds to 40 e^-/formula, which is associated with a hypothetical closed-shell $(Eu^{2+})_5(Gd^{3+})_2(Ge_6)^{16-}$ phase with the Ca_7Sn_6 structure. The

dx.doi.org/10.1021/ic2026413 | Inorg. Chem. 2012, 51, 3172–3178

closed-shell configuration of "$Eu_5Gd_2Ge_6$" is expected to generate a band gap. However, the oversimplified Zintl–Klemm formalism ignores the existence of R 5*d* orbitals and their dispersion characteristics around the E_F (see Figure 6). The significant hybridization among the R *d*-states and the Ge *p*-states leads to the obvious R–R and R–Ge bonding interactions around the E_F (Figure 6), eliminating the expected gap and resulting instead in a pseudo-gap for "$Eu_5Gd_2Ge_6$". The contribution from the metal *d* orbitals and their bonding with the neighboring main-group-element *p* orbitals around E_F were used to explain metallic properties of the nominally electron-precise Ca_5Ge_3 compound and related Cr_5B_3-type phases.[45] The Fermi level of $Eu_{6.5}Gd_{0.5}Ge_6$ is observed at 0.07 eV ($x = 0.5$) and lies below the pseudo-gap, confirming its electron-poor character. The questions that can be asked are: (i) What is the effect of this lower VEC on bonding? and (ii) Why does its phase range seem to be limited?

For the Ge_2^{6-} dimer of the electron-precise R_7Ge_6 phase, the molecular orbitals (MOs) can be simply written as $\sigma_s^2\sigma_s^{*2}\sigma_p^2\pi_p^4\pi_p^{*4}\sigma_p^{*0}$. The π_p and π_p^* orbitals have a relatively small contribution to the dimer bonding, because the π interactions are relatively weak and the *p* orbitals contributing to these π MOs are strongly involved into the R–Ge interactions. Still, the π_p^* states of the Ge2–Ge3 dimer are clearly seen in the COHP plot (see Figure 6). It is worth mentioning that, since the Ge2–Ge3 dimer resides within the $^2_\infty[R_5Ge_4]$ slab, which is a building block for the R_5X_4 phases; its bonding character is similar to that of the X–X dimers in R_5X_4.[5] However, a different electron count yields different population of the *p*-states for the dimers: in $Eu_{6.5}Gd_{0.5}Ge_6$, E_F falls into the π_p^* states, whereas in R_5X_4, e.g., Gd_5Ge_4, E_F is pushed up into the σ_p^* states, because of an electron excess.

The bonding within the Ge_4 tetramer can be also analyzed in terms of individual Ge1–Ge4 and Ge4–Ge4 interactions (see Figure 6). However, there is a striking difference, especially in the area of the σ_s states, between these dimers and Ge2–Ge3. Namely, there are four σ_s peaks for the Ge1–Ge4 and Ge4–Ge4 bonds and only two σ_s peaks for the Ge2–Ge3 dimer. This difference is due to the fact that the Ge1–Ge4 and Ge4–Ge4 dimers are fused into a tetramer with the local C_{2h} symmetry. The resulting MOs for the σ_s and π_p interactions are shown in Figure 7. Interestingly, the σ_s, σ_s^*, π_p, and π_p^* states will have different sequences for the Ge1–Ge4 and Ge4–Ge4 dimers: bonding, bonding, antibonding, and antibonding for the Ge1–Ge4 dimers and bonding, antibonding, bonding and antibonding for the Ge4–Ge4 ones. These trends are clearly seen in the COHP plots in the range from −10 eV to −6 eV, where the *s* states dominate (see Figure 6). As for the π states, these features are washed out due to the weaker π interactions and also due to a significant mixing with the *d* orbitals of neighboring R atoms. Still, an antibonding character of the Ge1–Ge4 interactions above −0.8 eV is visible and stems from the π_p^* states.

Thus, the Ge–Ge bonds would promote a lower VEC, which would minimize the population of the π_p^* states. However, a VEC reduction would have somewhat different effects on different bonds. A lower VEC of 38 e^-, as in pure Eu_7Ge_6, will strengthen the Ge1–Ge4 interactions within the tetramer but will have almost no effect on the Ge4–Ge4 within the tetramers. In fact, it appears that the overall bonding within the tetramer can tolerate even a slightly higher VEC as in $Eu_{6.5}Gd_{0.5}Ge_6$ without much penalty. A lower VEC will benefit

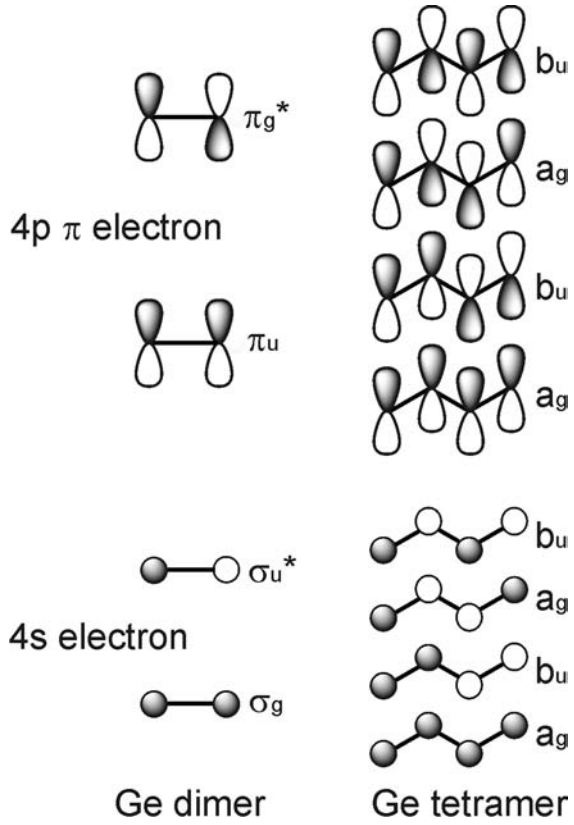

Figure 7. Schematic molecular orbital diagram for 4*s* and 4*p* π electrons of a Ge_2 dimer (Ge2–Ge3) and zigzag Ge_4 tetramer (Ge1–Ge4–Ge4–Ge1).

most the Ge2–Ge3 dimer as fewer of its strongly antibonding π_p^* states will be populated. On the other hand, any decrease in the VEC, achieved through a lower Gd amount or Gd absence, will weaken the bonding R–Ge and R–R. In addition, the Gd-free Eu_7Ge_6 phase is compositionally close to the EuGe binary, which contains infinite Ge zigzag chains with the Ge–Ge bonding resembling that of the Ge tetramers in $Eu_{6.5}Gd_{0.5}Ge_6$. Thus, a larger VEC achieved through Gd substitution is required to stabilize the Ca_7Sn_6-type structure. On the other hand, an even larger VEC (beyond $x = 0.5$ of Gd) appears to promote formation of the Gd_5Si_4-type R_5Ge_4 phases, which offer more of the strong R–R bonds in the presence of weaker Ge–Ge dimers. In summary, one may argue that there is a fine balance between the VEC and bonding in $Eu_{6.5}Gd_{0.5}Ge_6$ and the VEC of 38.5 e^- is optimal for the overall bonding.

■ CONCLUSIONS

The electron-poor $Eu_{6.5}Gd_{0.5}Ge_6$ polar intermetallics phase adopts the orthorhombic Ca_7Sn_6-type structure and it can be considered as an intergrowth of the Gd_5Si_4-type (*Pnma*) R_5Ge_4 and FeB-type (*Pnma*) RGe phases. The slab-surface R2 site is expected to preferentially accommodate Gd, based on the geometric and electronic factors. The Ca_7Sn_6-type $(Eu,Gd)_7Ge_6$ phase survives in a narrow composition range. Its stability and composition represents a compromise between the VEC, bonding, and competition from the binary EuGe and pseudo-binary $(Eu,Gd)_5Ge_4$ phases. $Eu_{6.5}Gd_{0.5}Ge_6$ provides an attractive way to develop new compounds by integrating the $^2_\infty[R_5X_4]$ slabs with other symmetry-compatible building blocks. Furthermore, considering the structural similarity of the

dx.doi.org/10.1021/ic2026413 | *Inorg. Chem.* 2012, 51, 3172–3178

R_5X_4 and R_7X_6 structures, we may anticipate structural transformations and concomitant changes in the physical properties via controlling the cleavage/formation of the X−X dimers.

■ ASSOCIATED CONTENT

Supporting Information

Single-crystal crystallographic files in CIF format, and the structural models for Eu_6GdGe_6. This material is available free of charge via the Internet at http://pubs.acs.org.

■ AUTHOR INFORMATION

Corresponding Author

*Tel.: +1 905 525 9140, ext 27796. Fax: +1 905 521 2773. E-mail: mozhar@mcmaster.ca.

Notes

The authors declare no competing financial interest.

■ ACKNOWLEDGMENTS

This work was supported by Discovery Grant from the Natural Sciences and Engineering Research Council of Canada and by a grant from the ACS Petroleum Research Fund.

■ REFERENCES

(1) Pecharsky, V. K.; Gschneidner, K. A. *Phys. Rev. Lett.* **1997**, *78*, 4494.
(2) Choe, W.; Pecharsky, V. K.; Pecharsky, A. O.; Gschneidner, K. A.; Young, V. G.; Miller, G. J. *Phys. Rev. Lett.* **2000**, *84*, 4617.
(3) Pecharsky, V. K.; Holm, A. P.; Gschneidner, K. A.; Rink, R. *Phys. Rev. Lett.* **2003**, *91*, 197204.
(4) Magen, C.; Arnold, Z.; Morellon, L.; Skorokhod, Y.; Algarabel, P. A.; Ibarra, M. R.; Kamarad, J. *Phys. Rev. Lett.* **2003**, *91*, 207202.
(5) Mozharivskyj, Y.; Choe, W.; Pecharsky, A. O.; Miller, G. J. *J. Am. Chem. Soc.* **2003**, *125*, 15183.
(6) Wu, L. M.; Kim, S. H.; Seo, D. K. *J. Am. Chem. Soc.* **2005**, *127*, 15682.
(7) Tobash, P. H.; Bobev, S. *J. Am. Chem. Soc.* **2006**, *128*, 3532.
(8) Tobash, P. H.; Bobev, S.; Thompson, J. D.; Sarrao, J. L. *Inorg. Chem.* **2009**, *48*, 6641.
(9) Misra, S.; Miller, G. J. *J. Am. Chem. Soc.* **2008**, *130*, 13900.
(10) Svitlyk, V.; Campbell, B. J.; Mozharivskyj, Y. *Inorg. Chem.* **2009**, *48*, 10364.
(11) Kozlov, A. Y.; Pavlyuk, V. V.; Davydov, V. M. *Intermetallics* **2004**, *12*, 151.
(12) Holtzberg, F.; Gambino, R. J.; McGuire, T. R. *J. Phys. Chem. Solids* **1967**, *28*, 2283.
(13) Smith, G. S.; Tharp, A. G.; Johnson, W. *Acta Crystallogr.* **1967**, *22*, 940.
(14) Yao, J.; Wang, P.; Mozharivskyj, Y. *Chem. Mater.* **2012**, DOI: 10.1021/cm203148e.
(15) Sears, V. F. *Neutron News* **1992**, *3*, 26.
(16) Hunter, B. A. *Int. Union Crystallogr. Comm. Powder Diffr. Newsl.* **1998**, *20*, 21.
(17) STOE; 2.05 ed.; STOE & Cie GmbH: Darmstadt, Germany, 2004.
(18) Sheldrick, G. M. *Acta Crystallogr., Sect. A: Found Crystallogr.* **2008**, *64*, 112.
(19) Sheldrick, G. M. *SHELXL*; University of Göttingen: Göttingen, Germany, 1997.
(20) Yao, J.; Mozharivskyj, Y. *Z. Anorg. Allg. Chem.* **2011**, *637*, 2039.
(21) Lambrecht, W. R. L.; Andersen, O. K. *Phys. Rev. B* **1986**, *34*, 2439.
(22) Jepsen, O.; Burkhardt, A.; Andersen, O. K.; The TB-LMTO-ASA Program, 4.7 ed.; Max-Planck-Institut fr Festkrperforschung: Stuttgart, Germany, 1999.
(23) Andersen, O. K.; Jepsen, O. *Phys. Rev. Lett.* **1984**, *53*, 2571.
(24) Andersen, O. K.; Jepsen, O.; Glotzel, D. In *Highlights of Condensed-Matter Theory*; Bassani, F., Fumi, F., Tosi, M. P., Eds.; Elsevier: Amsterdam, 1985; p 59.
(25) Blöchl, P. E.; Jepsen, O.; Andersen, O. K. *Phys. Rev. B* **1994**, *49*, 16223.
(26) Shannon, R. D. *Acta Crystallogr., Sect. A: Cryst. Phys. Diffr. Theor. Gen. Crystallogr.* **1976**, *32*, 751.
(27) Palenzona, A.; Manfrinetti, P.; Fornasini, M. L. *J. Alloys Compd.* **2000**, *312*, 165.
(28) Palenzona, A.; Manfrinetti, P.; Fornasini, M. L. *J. Alloys Compd.* **2002**, *345*, 144.
(29) Bobev, S.; Bauer, E. D.; Thompson, J. D.; Sarrao, J. L.; Miller, G. J.; Eck, B.; Dronskowski, R. *J. Solid State Chem.* **2004**, *177*, 3545.
(30) Schobingerpapamantellos, P.; Demooij, D. B.; Buschow, K. H. J. *J. Alloys Compd.* **1992**, *183*, 181.
(31) Koch, E.; Fischer, W. *Z. Kristallogr.* **1996**, *211*, 251.
(32) Gordon, J. M. *Eur. J. Inorg. Chem.* **1998**, *1998*, 523.
(33) James, A. M.; Lord, M. P. *Macmillan's Chemical and Physical Data*; Macmillan: London, UK, 1992.
(34) Harmon, B. N.; Freeman, A. J. *Phys. Rev. B* **1974**, *10*, 1979.
(35) Roeland, L. W.; Cock, G. J.; Muller, F. A.; Moleman, A. C.; McEwen, K. A.; Jordan, R. G.; Jones, D. W. *J. Phys. F* **1975**, *5*, L233.
(36) Yeung, I.; Roshko, R. M.; Williams, G. *Phys. Rev. B* **1986**, *34*, 3456.
(37) Behrendt, D. R.; Legvold, S.; Spedding, F. H. *Phys. Rev.* **1958**, *109*, 1544.
(38) Schobinger-Papamantellos, P. *J. Magn. Magn. Mater.* **1982**, *28*, 97.
(39) Prokhnenko, O.; Arnold, Z.; Kamarad, J.; Ritter, C.; Isnard, O.; Kuchin, A. *J. Appl. Phys.* **2005**, *97*, 113909.
(40) Banerjee, B. K. *Phys. Lett.* **1964**, *12*, 16.
(41) Zintl, E. *Angew. Chem.* **1939**, *52*, 1.
(42) Schäfer, H.; Eisenmann, B.; Müller, W. *Angew. Chem., Int. Ed.* **1973**, *12*, 694.
(43) *Chemistry, Structure, and Bonding of Zintl Phases and Ions*; Kauzlarich, S. M. ed.; VCH Publishers: New York, 1996.
(44) Albert, K.; Meyer, H. J.; Hoffmann, R. *J. Solid State Chem.* **1993**, *106*, 201.
(45) Mudring, A. V.; Corbett, J. D. *J. Am. Chem. Soc.* **2004**, *126*, 5277.